ChemPubSoc Europe

DOI: 10.1002/slct.201601362

Chemistry SELECT Full Papers

Catalysis

Morphology Control and Electro catalytic Activity towards Oxygen Reduction of Peptide-Templated Metal Nanomaterials: A Comparison between Au and Pt

Qiannan Wang,[a] Zhenghua Tang,*[a, b] Likai Wang,[a] Hongyu Yang,[a] Wei Yan,[a] and Shaowei Chen[a, c]

Peptide templated noble metal nanomaterials have been considered as an emerging type of nanomaterials, which can find widespread catalytic applications in a variety of organic reactions. However, their electrocatalytic properties remained largely unexplored. Herein, peptide R5 templated Au and Pt nanomaterials were fabricated and employed as catalysts for oxygen reduction reaction (ORR). By tuning the metal-to-peptide ratio, different shaped Au and Pt nanomaterials were obtained and observed by TEM measurements. With lower metal-to-peptide ratios, spherical nanoparticles were obtained for both Au and Pt, while higher metal-to-peptide ratios led to the formation of nanoribbons and/or networked nanochains. All the Au and Pt nanomaterials demonstrated good ORR activity, while R5-Au-90 and R5-Pt-90 exhibited the best performance in their own series. Morphological effects of Au and Pt nanomaterials upon ORR were established. R5-Pt-90 exhibited comparable activity with Pt/C, as manifested by the onset potential, specific activity as well as the long-term durability. The findings can shed light on rational design of peptide templated noble metal nanomaterials with desired morphology and optimized electrochemical properties as catalyst for electrochemical reactions.

Introduction

In the past decade, significant advances have been achieved on fabricating noble metal nanomaterials (e.g. Au and Pt) as catalysts with controllable size, shape, morphology and composition.[1–3] Among all kinds of noble metal nanostructures, Au and Pt nanomaterials have been attracting continuous research attentions, thanks to their robust stability, easy fabrication, excellent optical and electrochemical properties as well as the readily modifiable surface functionalities. For instances, Au nanoparticles have demonstrated excellent catalytic activity towards CO oxidation,[4] 4-nitrophenol reduction,[5] selective oxidation and hydrogenation of organic molecules,[6] as well as electrochemical reactions such as oxygen electroreduction.[7–9] Meanwhile, superior catalytic activity of Pt nanomaterials have been found in a variety of reactions including 2-propanol oxidation,[10] CO oxidation,[11] and oxygen reduction reaction (ORR).[12] Notably, recent reports show that Pt nanoparticles with high-index surfaces which expose a significant amount of low-coordinated atomic edge sites exhibited exceptional catalytic activity for ORR.[13–14] Notably, ORR is a critical reaction determining the efficiency of fuel cells and lithium-air batteries,[15–16] which can deliver and store reliable and cost effective environmental friendly energy to tackle the global energy crisis. However, such efficiency is mainly governed by the catalysts (e.g. Pt/C) employed in ORR, consequently, developing stable and active Pt or non-Pt based nanostructured catalyst is the key to improve the efficiency.[17–27]

To fully realize the catalytic potentials of the metallic nanomaterials, precise structural control at the atomic level is urgent and quite necessary. Moreover, to achieve enhanced stability, surface ligands or templates have been extensively employed to protect or stabilize the metal core. Such ligands or templates include thiol molecules,[28–29] DNA,[30] protein,[31] dendrimer[32] as well as peptide.[33–34] Peptides are polymeric molecules made of amino acids, with 20 natural amino acid residues, the structure of the peptides can be easily fine tuned and versatile functionalities are endorsed through amino acid residues. In conjunction with distinctive self-assembly properties and surface recognition capability, peptide has become one of the most promising ligands to direct the fabrication of noble metal nanomaterials.[34–35] Peptide based metal nanomaterials can be easily prepared in environmental friendly conditions (e.g. water as solvent, room temperature), and peptide can direct the nuclei growth and material formation

[a] Q. Wang, Prof. Z. Tang, L. Wang, H. Yang, W. Yan, Prof. S. Chen
New Energy Research Institute, School of Environment and Energy
South China University of Technology, Guangzhou Higher Education Mega Centre
Guangzhou, Guangdong 510006, P. R. China
E-mail: zhht@scut.edu.cn
[b] Prof. Z. Tang
Guangdong Provincial Key Lab of Atmospheric Environment and Pollution Control, Guangdong Provincial Engineering and Technology Research Center for Environmental Risk Prevention and Emergency Disposal
South China University of Technology, Guangzhou Higher Education Mega Centre
Guangzhou 510006, P. R. China.
[c] Prof. S. Chen
Department of Chemistry and Biochemistry
University of California
1156 High Street, Santa Cruz, California 95064, United States.

Supporting information for this article is available on the WWW under http://dx.doi.org/10.1002/slct.201601262

hence precisely control the size, shape, morphology and subtle surface microstructures. For instances, by employing selected peptide molecule P7 A, ultrasmall Pt nanocrystals with monodisperse size and uniform morphology have been prepared by Huang group.[36] They also successfully demonstrated the formation of single-twinned right bipyramid and 111-bipyramid[37] as well as platinum nanocubes and nanotetrahedrons[38] by employing facet-specific peptide sequences.

Peptide R5, with a sequence of SSKKSGSYSGSKGSKRRIL, was first discovered as a protein composition of cell walls from the diatom *Cylindrathica fusiformis*.[39] Interestingly, R5 possesses self-assembly properties, as the *C*-terminal RRIL motif can drive the formation of self-assembly templates. It has been documented that R5 can regulate and direct the formation of silica, titanium phosphate and titanium dioxide under mild conditions.[40–42] Recently, Knecht group reported the fabrication of R5 templated Pd nanomaterials as catalysts for both stille coupling reaction and 4-nitrophenol reduction.[43] The metal surface area and the penetration depth within the peptide scaffold are the most two important factors that govern the catalytic activity.[43] Furthermore, structural control on R5 templated Pt and Au nanomaterials were achieved by Bhandri *et. al*, and both Pt and Au nanomaterials exhibited excellent reactivity towards olefin hydrogenation and 4-nitrophenol reduction.[44]

Despite the significant progresses have been made on R5 templated noble metal nanomaterials as catalysts, their electrocatalytic properties remained largely unexplored. The immediate questions appear as follows: Do these R5 templated noble metal nanomaterials possess electrocatalytic property? If so, as R5 can govern shape and morphology of the nanomaterials, how the shape/morphology affect the electrocatalytic activity? Furthermore, with different noble metals are employed, what is the electrocatalytic activity difference and is that possible to establish a correlation between the morphology of R5 templated different metal nanomaterials and their corresponding electrocatalytic activity eventually?

Herein, peptide R5 templated Au and Pt nanomaterials were fabricated and employed as catalysts for ORR. By tuning the metal-to-peptide ratio, different shaped Au and Pt nanomaterials were acquired. Interestingly, with lower ratios, spherical nanoparticles were obtained for both Au and Pt, while higher metal-to-peptide ratio led to the formation of nanoribbons and/or networked nanochains. All the Au or Pt nanomaterials with different morphologies demonstrated good activity toward ORR. R5-Au-90 and R5-Pt-90 exhibited the best activity among their own series of Au or Pt nanomaterials, respectively, in terms of onset potential, kinetic current density as well as number of electron transfer. Meanwhile, compared with R5-Au-90, R5-Pt-90 exhibited superior activity, as much larger kinetic current density and higher specific activity and mass activity were obtained. Notably, R5-Au-90 demonstrated markedly higher stability than R5-Pt-90.

Results and Discussion

Au and Pt nanomaterials were first fabricated separately by employing R5 as the template. For both Au and Pt, the molar ratio of metal-to-R5 were controlled as 30, 60, 90 and 120 (Denoted as R5-Au–X or R5-Pt–X, X is 30, 60, 90 and 120). The UV-visible absorbance spectra of the samples were shown in **Figure S1.** Nearly identical features were obtained for the R5-Au–X samples. One can see that, there is a small narrow absorbance peak at ~270 nm, which is probably from Au^{3+} ions.[45–46] Moreover, a very broad absorbance peak at wavelength higher than 500 nm can be easily identified, indicating relatively larger gold nanostructures[47] and bulky gold aggregates were probably formed.[45] Note that, the absorbance increased with the increasing of Au concentration. While for the R5-Pt–X samples, a featureless decay absorbance profile was obtained. Similar with Au, the absorption intensity increased with the amount of Pt, and the largest absorption was obtained from the R5-Pt-120 sample.

Next, the surface microstructures of the Au or Pt nanomaterials were examined by TEM measurements. As depicted in the Figure 1, nanoparticle networks or aggregates were observed for all the R5-Au–X samples, but the morphology of the Au nanomaterials changed with the variation of Au-to-R5 ratio. For R5-Au-30, besides a few aggregates, well-defined spherical particles dominated the sample. The average diameter of these spherical particles (**Figure S2**) were calculated as 4.89 ± 0.95 nm. With the increasing of Au concentration, more networked chains were observed, as shown in the samples of R5-Au-60 and R5-Au-90. One can see that, bulky nanoparticle aggregates were formed for the sample of R5-Au-120. The morphology change trend agrees well with the previous paper,[44] however, still some differences regarding the stability existed. Note that, in the previous report, black and blue precipitates formed immediately upon reduction for the samples of R5-Au-90 and R5-Au-120.[44] Herein, all the R5-Au–X samples can be stable for 1–2 days. The enhanced stability might be attributed to the different synthetic conditions resulted different materials. For Au materials, the precursor we employed is $KAuCl_4$ instead of $HAuCl_4$, upon reduction, the solution was aged for 1 h instead of stirring for 1 h.

The representative HR-TEM images of the R5-Pt–X samples can be found in Figure 2. Well-defined spherical particles can be found from the sample of R5-Pt-30, and based on more than 200 individual particles, the average diameter is calculated as 1.34 ± 0.26 nm (**Figure S3**). With the increasing of Pt concentration, networked chains or ribbons can be easily recognized. For the sample of R5-Pt-60, both spherical particles and nanoribbons exist simultaneously, while nanoribbons dominated in the sample of R5-Pt-90. Interestingly, for the sample of R5-Pt-120, networked nanochains with larger dimensions were observed. Interestingly, spherical nanoparticles were generated irrespective of Pt-to-R5 ratio in the previous report.[48] The discrepancy might originate from different synthetic conditions employed here. To generate a more concentrated solution for ORR test, the total volume employed was 2 mL instead of 3 mL in the previous paper, hence the

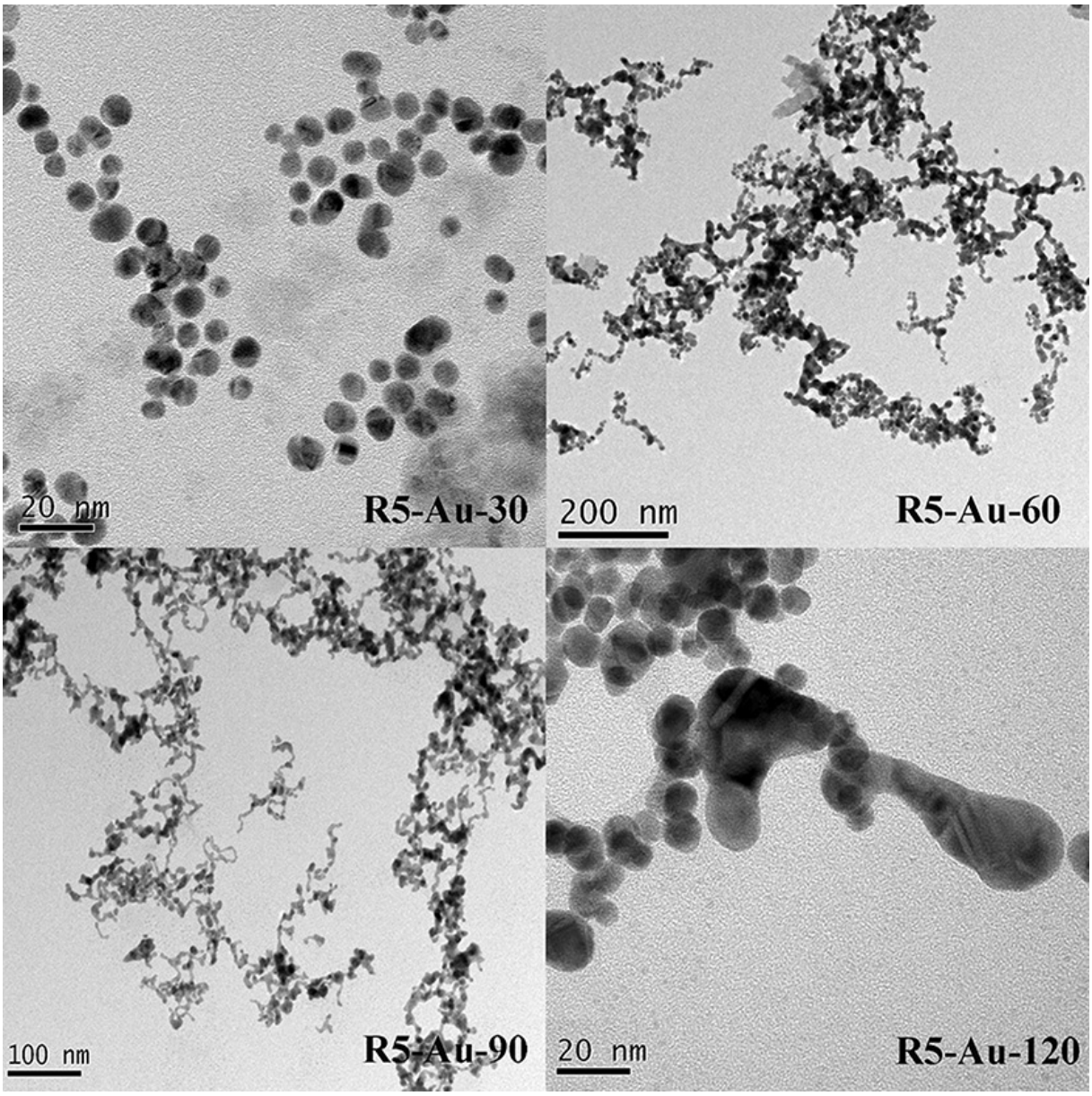

Figure 1. Representative HR-TEM images of R5-Au–X samples (X is the molar ratio of Au-to-R5, X = 30, 60, 90, and 120).

concentration of Pt and peptide R5 both increased. The reaction was also proceeded for 48 h here instead of 24 h in the previous paper. Note that higher concentration and longer reaction time are both favorable for the self-assembly process. This is probably why Pt nanoribbons and nanoparticle networks were formed in the present study. The appearance of networked chains or aggregates from Au nanomaterials and ribbons or networked chains from Pt nanomaterials were probably caused by the self-assembly properties of peptide R5. Note that, the C-terminal RRIL motif can drive R5 to form peptide scaffold, with metal ions entrapped in such scaffold, upon reduction, nanomaterials can be formed.[49] Meanwhile, with the increase of metal ion concentration, the metal-metal interaction enhanced, which impacted the nanomaterial formation process differently at various stages, subsequently, different shaped nanomaterials were formed. It is worth pointing out that, such template induced synthetic approach is quite common in nanomaterial synthesis. Crooks and coworkers have devoted tremendous efforts on fabrication of noble metal materials by employing a variety of dendrimers as template.[32, 50–52] For instances, Pt nanoparticles encapsulated by fourth generation dendrimer were prepared by Ye et al., and the resulting films were electrocatalytically active for ORR.[53] They also found that Au@Pt core-shell nanoparticles encapsulated in dendrimer possessed much higher ORR activity than Au or Pt nanoparticles encapsulated alone.[50]

Then the ORR activity of the Au and Pt nanomaterials were investigated. Table 1 summarizes the ORR activity of all the Au

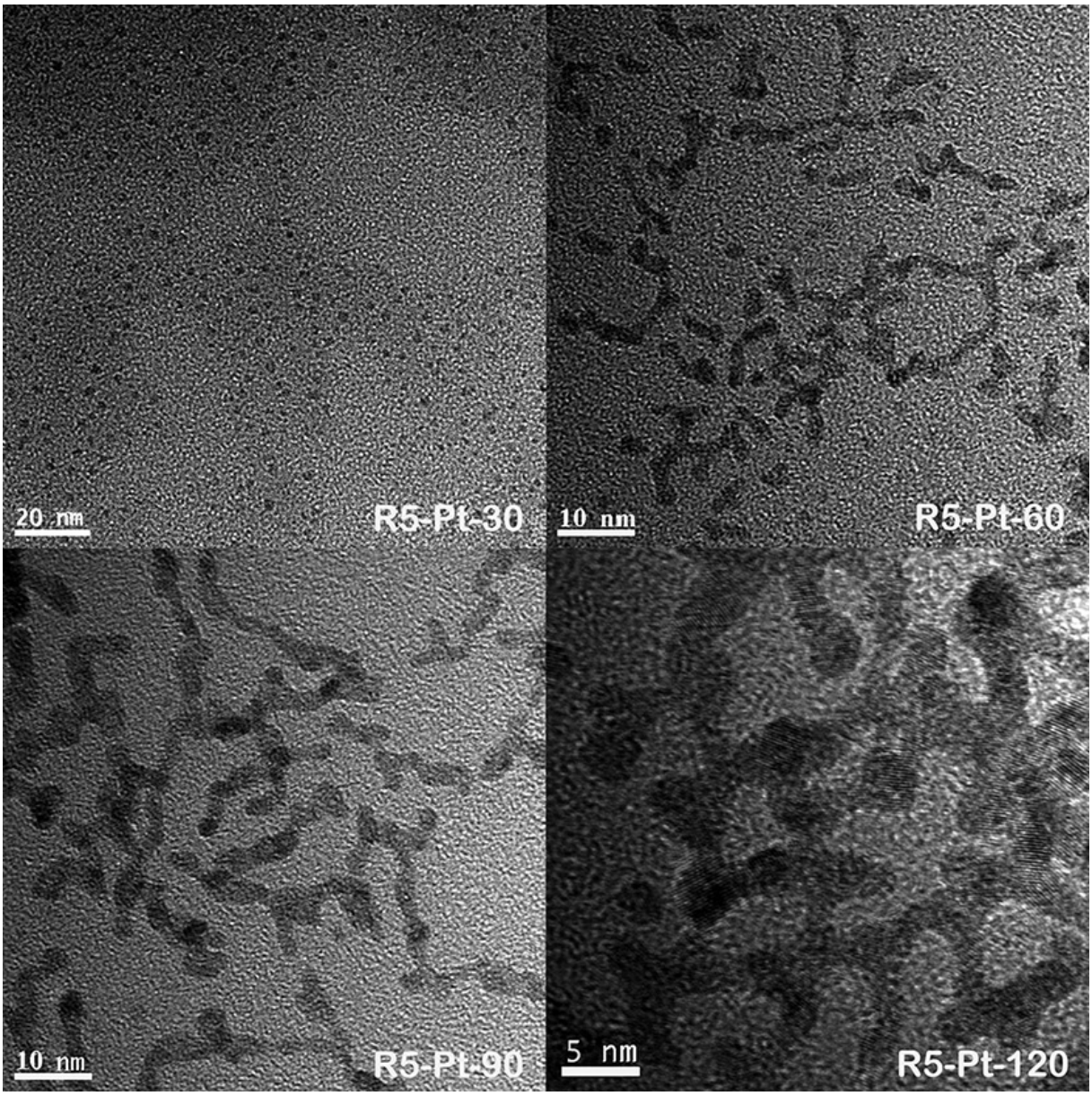

Figure 2. Representative HR-TEM images of R5-Pt–X samples (X is the molar ratio of Pt-to-R5, X = 30, 60, 90 and 120).

and Pt nanomaterials templated by R5 as well as Pt/C. Note that, for R5-Pt-30, as the onset potential (0.68 V) is below 0.80 V, the ORR current at 0.80 V is negligible, so the specific activity value is quite low which is not listed in Table 1. The electrocatalytic activities toward ORR were compared with CV and RRDE voltammetric measurements in oxygen-saturated 0.1 M KOH solution in the potential range of −0.04 V to +1.16 V. As shown in **Figures 3a** and **3d**, a sharp cathodic current peak from oxygen reduction appeared in CV curves, indicating both R5-Au–X and R5-Pt–X samples possessed effective ORR activity. The cathodic peak potentials were estimated as 0.58 V for R5-Au-30, 0.70 V for R5-Au-60, 0.79 V for R5-Au-90, 0.78 V for R5-Au-120, 0.60 V for R5-Pt-30, 0.85 V for R5-Pt-60, 0.88 V for R5-Pt-90, and 0.82 V for R5-Pt-120, respectively. R5-Au-90 outperforms other samples in the R5-Au–X series, while R5-Pt-90 exhibits the most positive cathodic peak potential in the series of R5-Pt–X. Notably, larger cathodic peak current density was also obtained for these two samples.

The ORR activity comparison of these Au or Pt nanomaterials was further probed by RRDE test. As shown in Figures 3b and 3e, for both R5-Au–X and R5-Pt–X, the ring current density is less than an order of magnitude of disk current density, suggesting that only a small amount of H_2O_2 as byproduct was produced for all the samples. Notably, the onset potential and kinetic disk current density of the Au and Pt nanomaterials vary drastically with different metal-to-peptide ratios. For both R5-Au–X and R5-Pt–X, the onset potential increased with the increasing of metal concentration. For

Table 1. Summary of the ORR activity of R5 templated Au and Pt nanomaterials including shape and morphology, E_{onset}, electron transfer numbers (n), electrochemically active surface area (ECSA) and specific activity at 0.8 V.

Sample	Shape and morphology	E_{onset} (V)	n Value	ECSA (cm^2)	Specific activity at 0.8 V (mA cm^{-2})
R5-Au-30	Sphere	0.82	3.22-3.70	0.14	0.19
R5-Au-60	Networked chain	0.85	3.60-3.80	0.50	0.21
R5-Au-90	Networked chain	0.90	3.68-3.87	0.85	0.25
R5-Au-120	Aggregates	0.88	3.62-3.82	0.76	0.22
R5-Pt-30	Sphere	0.68	2.25-3.12	0.20	–
R5-Pt-60	Sphere & Ribbon	0.88	3.20-3.76	0.30	0.53
R5-Pt-90	Ribbon	0.91	3.72-3.94	0.69	0.61
R5-Pt-120	Networked chain	0.85	3.56-3.87	0.65	0.51
Pt/C	–	0.93	3.93-3.95	1.72	0.62

instance, the onset potential is 0.82 V for R5-Au-30, 0.85 V for R5-Au-60 and 0.90 V for R5-Au-90. However, further increasing of Au concentration result in the decrease of the onset potential, as a value of 0.88 V was obtained for R5-Au-120. Similar trend was observed for the R5-Pt–X samples.

Moreover, the kinetic disk current density of the samples also followed the same order. The sample of R5-Au-90 and R5-Pt-90 exhibited the most positive onset potential of 0.90 V and 0.91 V (Figure 4a), as well as largest experimental disk current density of 2.22 mA cm^{-2} and 4.24 mA cm^{-2} (Figure 4b), respectively. The results agree well with the above CV measurements, further confirm that R5-Au-90 and R5-Pt-90 possessed the best activity in their own series. It is interesting to notice that, the disk current density of the R5-Pt–X samples is generally higher than that of R5-Au–X samples. For example, the lowest disk current density from R5-Pt–X series is 2.21 mA/cm^2 and 2.23 mA/cm^2 at 0 V, both of which is almost identical with the highest value of 2.22 mA/cm^2 from R5-Au-90 sample in the R5-Au–X series.

It is worth noting that, small cathodic peaks exhibited in the polarization curves of LSV measurements for both Au (Figure **3b, 4b** and **4c**) and Pt (Figure **3e, 4b** and **4d**) nanomaterials. For Au nanomaterials, there are two anionic peak at ~0.7 V and ~0.5 V, where the former one can be attributed to the formation of HO_2^- on Au(111) and Au(100) facets and the latter is probably assigned to the further reduction of HO_2^- to OH^-.[8, 54] Similar phenomenon can be found for Pt nanomaterials, the two peak at ~0.75 V and ~0.45 V are attributed to the formation of HO_2^- and OH^- on Pt(111) facet, respectively.[55]

Furthermore, based on the RRDE voltammetric measurements, the number of electron transfer (n) and the H_2O_2 yield can be calculated[56] by

$$\mathbf{n} = \frac{4^* I_d}{I_d + I_r/N}$$

$$H_2O_2 = \frac{200 I_r/N}{\frac{I_r}{N} + I_d}$$

In the equations, I_d is the disk current, I_r is the ring current, and N is the RRDE collection efficiency (0.37). Figure **3c** presents the n values and H_2O_2 yields of the R5-Au–X samples. Again, R5-Au-90 stood out as the best sample, as the n value was 3.68 - 3.86 and the corresponding H_2O_2 yield was $<20\%$ within the wide potential range of 0 V to +0.80 V. From Figure **3f**, one can find the n values and the H_2O_2 yields for the R5-Pt–X samples. R5-Pt-90 also outperforms other samples, and the n values were 3.74-3.94 while the corresponding H_2O_2 yield was less than 10%.

Since R5-Au-90 and R5-Pt-90 are both the best sample among their own series, the catalytic performance between them were then compared by Cyclic and RRDE voltammetric measurements. As depicted in **Figure S4**, the CV and LSV curves of the GCE electrode modified by peptide R5 show that it barely has ORR activity, as the onset potential is about ~0.62 V. **Figure S5** shows the CV curves and RRDE voltammograms of the GCE electrode modified by the two samples and Pt/C in 0.1 M KOH solution saturated with N_2 or O_2. In the presence of oxygen, a well defined peak attributed to oxygen reduction at ~0.90 V can be identified easily, indicating both samples possess effective ORR activity. From the CV curve shown in Figure **4a**, one can see that the onset potential of R5-Pt-90 is slightly larger than R5-Au-90 (0.91 V vs 0.90 V, listed in Table 1). Meanwhile, the disk current density of R5-Pt-90 is almost twice that of R5-Au-90 (Figure **4b**), and the ring current density of R5-Pt-90 is about three times of R5-Au-90. Consequently, according the equations for calculating the electron transfer number and H_2O_2 yield, the electron transfer number of R5-Pt-90 is higher than that of R5-Au-90 (3.74-3.94 vs 3.68-3.86, listed in Table 1), while the yield of H_2O_2 (5.94% for R5-Pt-90 vs 15.85% for R5-Au-90 at 0.5 V) is much lower, both of which suggest that R5-Pt-90 possessed higher catalytic activity for ORR than R5-Au-90.

The RRDE voltammograms of R5-Au-90 and R5-Pt-90 acquired in 0.1 M KOH solution with different rotation rates are shown in Figures 4c and 4d. One can see that, for both samples, the voltammetric current increased with the increasing of the rotation rate. The corresponding Koutecky-Levich (K–L) plots of R5-Au-90 and R5-Pt-90 were shown in Figures 4e and 4f respectively. Note that, in the potential range of 0.60 V-0.80 V, excellent linearity with very consistent slope were acquired for both samples, indicating both R5-Au-90 and R5-Pt-90 catalyze the oxygen reduction with a first order reaction kinetics. The K–L plots of the other Au and Pt samples can be found in Figure S6. Based on K–L plots, the electron transfer number n can also be calculated (Table S2).[26] As summarized in Table S2, the calculated n values were either close or in the range of the n values obtained from RRDE measurements. Moreover, the corresponding Tafel plots of R5-Au-90, R5-Pt-90 and Pt/C that obtained from K–L analysis of the RRDE can be found in Figure 5. The calculated Tafel slope is 69.8 mV/dec for R5-Pt-90, 94.7 mV/dec for R5-Au-90 and 64.2 mV/dec for Pt/C. One may notice that, the Tafel slope of R5-Pt-90 is quite close with Pt/C, indicating that a similar mechanism was adopted. Note that, by using Pt/C as catalyst, it has been well recognized

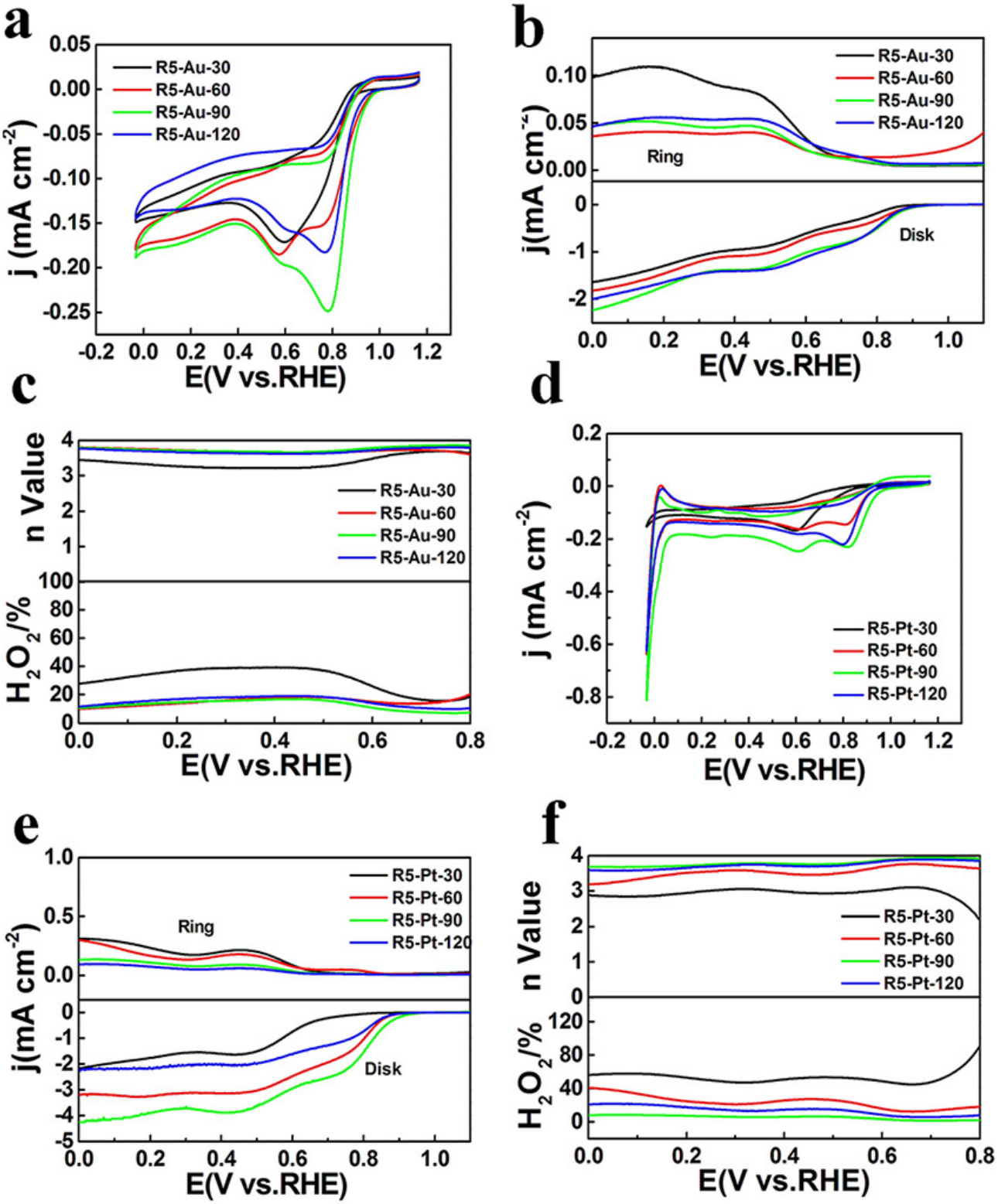

Figure 3. The electrochemical performance of the glassy carbon electrode (GCE) modified with 80 μg/cm^2 R5-Au–X or R5-Pt–X in O_2-saturated 0.1 M KOH solution: (a), (d) Cyclic and (b), (e) Rotating disk electrode (RDE) voltammograms, at a rotation speed of 2500 rpm with 10 mV/s potential sweep rate, (c), (f) plots of number of electron transfer and H_2O_2 (%) yield, respectively.

that the first electron transfer to oxygen molecule is the rate determining step.[17, 57] Interestingly, the Tafel slope of R5-Au-90 is much higher than that of Pt/C, suggesting a different mechanism.[18, 25] The R5-Au-90 probably takes a pseudo two

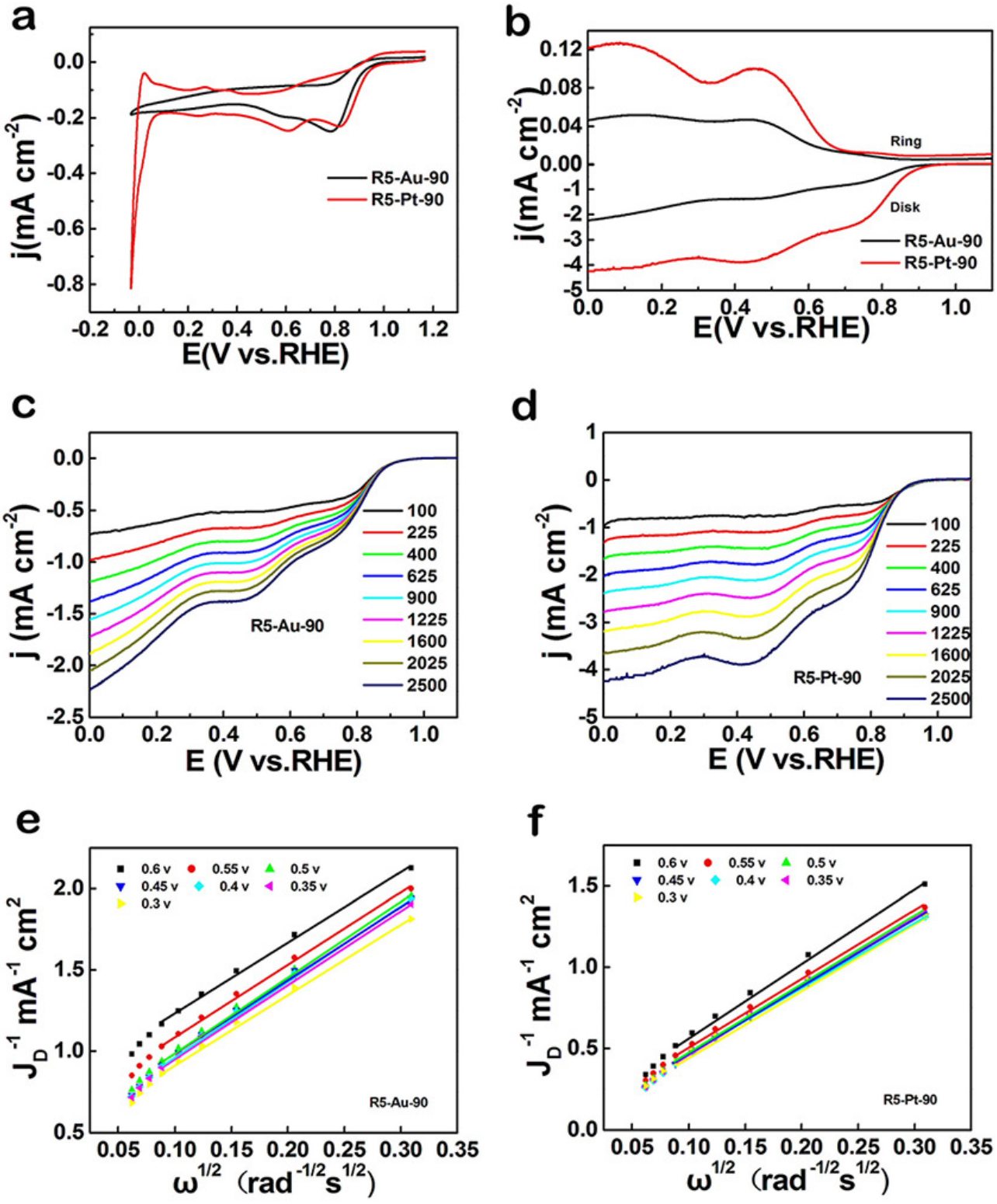

Figure 4. The comparison of the electrocatalytic performance of the GCE modified with 80 μg/cm^2 R5-Au-90 and R5-Pt-90 in O_2-saturated 0.1 M KOH solution: (a) Cyclic and (b) RRDE voltammograms at the 2500 rpm, the LSV curves of R5-Au-90 (c) and R5-Pt-90 (d) at the rotation rates of 100 to 2500 rpm, the corresponding Koutecky-Levich (K–L) plots of R5-Au-90 (e) and R5-Pt-90 (f) at different potentials.

electron reaction pathway. With all the above results combined, clearly one can see the ORR activity of R5-Pt-90 is higher than R5-Au-90, within the context of onset potential, kinetic current density, number of electron transfer and yield of H_2O_2. The

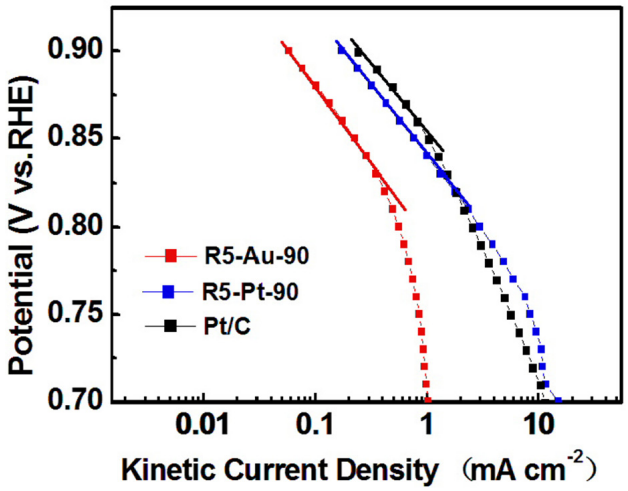

Figure 5. The corresponding Tafel plots of R5-Au-90, R5-Pt-90 and Pt/C, obtained from the Koutecky-Levich (K–L) analysis of the RRDE voltammograms (Figures 4c and 4d).

catalyst loading as well as their corresponding metal mass loading of each sample can be found in Table S1. Moreover, by normalizing the kinetic currents to the corresponding metal mass, the calculated mass activity is 11.1 A/g for R5-Au-90, 56.2 A/g for R5-Pt-90 and 159.4 A/g for Pt/C at 0.8 V.

However, the long-term stability of R5-Au-90 is greater than that of R5-Pt-90, attested by the chronoamperometric measurements for 35000 s (Figure S7). The cathodic current of the R5-Au-90 catalyst exhibited a loss of 25% of the initial value after more than 9 h' s continuous operation, whereas R5-Pt-90 only retained about 55% (45% loss) of its initial current under the same conditions. Note that, for both R5-Au-90 and R5-Pt-90, the onset potential remained almost constant after cycling for 3 times (Figure S8).

To elucidate the physical origin of the different ORR activities of the R5-Au–X and R5-Pt–X samples, the electrochemically active surface area (ECSA) tests (Figure S9) were conducted for all the samples.[58–59] Based on the CV curves in Figure S9, the ECSA value of each sample was calculated by

$$ECSA[cm^2] = Q\ [\mu C]/A$$

In the equation, A is the quantity of electricity per unit area for polycrystalline Au (400 μC cm^{-2}) or Pt (210 μC cm^{-2}) respectively. The ECSA values of all the samples are summarized in Table 1. The ECSA value of R5-Au-90 (0.85 cm^2) or R5-Pt-90 (0.69 cm^2) is higher than other samples in their own series, respectively. The specific activity (SA) was then calculated, and as shown in Table 1, R5-Au-90 possessed the highest value of 0.25 mA cm^{-2} in the R5-Au–X series, while R5-Pt-90 exhibited the largest value of 0.61 mA cm^{-2} in the R5-Pt–X series. One may notice that, the specific activity of R5-Pt–X is generally higher than that of R5-Au–X samples. Unfortunately, most of the samples possessed lower SA value than Pt/C, however, for the sample of R5-Pt-90, the SA value is almost identical with Pt/C, indicating a comparable activity.

One may notice that, peptide R5 probably block some catalytically active sites. Note that, the ECSA value decreased with the increasing of metal-to-R5 ratio in both R5-Au–X and R5-Pt–X series. R5-Au-90 and R5-Pt-90 possessed the highest value among their own series, thus bear the best ORR activity correspondingly. For R5-Au-120 and R5-Pt-120, even if less amount of peptide was employed, heavy aggregation was observed which significantly lowered the ECSA value.

It can be concluded that the functionality of peptide R5 actually plays an important role in influencing the ORR activity. Firstly, it is the capping agent which stabilizes the nanomaterials and block some catalytically active sites as well. With the increasing of metal loading, the more exposed surface without R5 capping facilitated the metal-metal interaction, which led to characteristic structure or aggregates. Secondly and more importantly, the self-assembly property of peptide R5 results in formation of different shaped nanomaterials, which ultimately triggered the drastically different ORR activity.

It is worth noting that, quite a few examples have been reported on the shape effects of Au or Pt nanoparticles upon ORR. Hernandez et al. found that the ORR activity is particularly sensitive with Au(100) surface, and cubic Au nanoparticles showed much better electrocatalytic activity than spherical nanoparticles or gold nanorods.[60] With carbon-black powder as support, Erikson *et al.* found that the highest specific activity was achieved on Au nanocubes but not octahedral or spherical particles.[61] Similarly, Pt nanocubes exhibited superior electrocatalytic capability toward ORR than other Pt structures including nanotubes, spherical particles, crystal aggregates as well as other morphologies.[62–65] Herein, R5-Au-90 exhibited the best activity among the R5-Au-90 series, which is due to the effective surface area of networked chain is larger than spherical particles and nanoparticle aggregates. Such shape effects were further manifested by the ORR activity of the R5-Pt-90 sample. The nanoribbons possess much larger effective surface area than spherical particles or networked chain structures. Although it is extremely difficult to achieve precise morphological control of Au or Pt nanomaterials by employing peptide as template, however, peptide based method highlights the merits of facile preparation, environmental friendly synthetic conditions as well as degradable properties of such catalysts. To the best of our knowledge, this is the first systematic ORR activity study of noble metal nanomaterials with peptide as template to control the shape and morphology, and the comparison example between Au and Pt nanomaterials has been successfully set.

Conclusions

In summary, peptide R5 was employed as a template to fabricate both Au and Pt nanomaterials with different shape and morphologies. The morphological control was governed and achieved by the self-assembly properties of peptide R5. All the R5 templated Au and Pt nanomaterials demonstrated good catalytic activity for ORR. For the R5-Au–X series, R5-Au-90 with networked chains demonstrated best activity than spherical particles or aggregates, while for the R5-Pt–X series, R5-Pt-90

with nanoribbons possessed the optimal ORR performance, superior than spherical particles and networked chains. Notably, R5-Pt-90 exhibited better ORR activity than R5-Au-90, while R5-Au-90 showed markedly higher long-term stability than R5-Pt-90. The findings can shed light on rational design of peptide templated noble metal nanomaterials with desirable surface structure and optimized electrocatalytic properties for electrochemical reactions.

Acknowledgements

Z. H. T acknowledges financial support from Project of Public Interest Research and Capacity Building of Guangdong Province (2015 A010105009), Guangdong Innovative and Entrepreneurial Research Team Program (No. 2014ZT05N200), Guangdong Natural Science Funds for Distinguished Young Scholars (No. 2015 A030306006) and the National Natural Science Foundation of China (No. 21501059).

Keywords: Au nanomaterials · Morphology control · Oxygen electroreduction · Peptide R5 · Pt nanomaterials

[1] N. R. Shiju, V. V. Guliants, *Appl. Catal. A: General* **2009**, *356*, 1–17.
[2] K. An, G. A. Somorjai, *ChemCatChem* **2012**, *4*, 1512–1524.
[3] Y. Li, G. A. Somorjai, *Nano Lett.* **2010**, *10*, 2289–2295.
[4] A. A. Herzing, C. J. Kiely, A. F. Carley, P. Landon, G. J. Hutchings, *Science* **2008**, *321*, 1331–1335.
[5] Y. Li, Z. Tang, P. N. Prasad, M. R. Knecht, M. T. Swihart, *Nanoscale* **2014**, *6*, 3165–3172.
[6] Y. Zhu, H. Qian, M. Zhu, R. Jin, *Adv. Mater.* **2010**, *22*, 1915–1920.
[7] W. Chen, S. Chen, *Angew. Chem., Int. Ed.* **2009**, *48*, 4386–4389.
[8] A. Sarapuu, M. Nurmik, H. Mändar, A. Rosental, T. Laaksonen, K. Kontturi, D. J. Schiffrin, K. Tammeveski, *J. Electroanal. Chem.* **2008**, *612*, 78–86.
[9] H. Erikson, G. Jürmann, A. Sarapuu, R. J. Potter, K. Tammeveski, *Electrochim. Acta* **2009**, *54*, 7483–7489.
[10] S. Mostafa, F. Behafarid, J. R. Croy, L. K. Ono, L. Li, J. C. Yang, A. I. Frenkel, B. R. Cuenya, *J. Am. Chem. Soc.* **2010**, *132*, 15714–15719.
[11] H. Borchert, D. Fenske, J. Kolny-Olesiak, J. Parisi, K. Al-Shamery, M. Bäumer, *Angew Chem., Int. Ed.* **2007**, *46*, 2923–2926.
[12] J. Wu, H. Yang, *Acc. Chem. Res.* **2013**, *46*, 1848–1857.
[13] S. Liu, N. Tian, A.-Y. Xie, J.-H. Du, J. Xiao, L. Liu, H.-Y. Sun, Z.-Y. Cheng, Z.-Y. Zhou, S.-G. Sun, *J. Am. Chem. Soc.* **2016**, *138*, 5753–5756.
[14] G. A. Attard, A. Brew, J.-Y. Ye, D. Morgan, S.-G. Sun, *ChemPhysChem* **2014**, *15*, 2044–2051.
[15] M. K. Debe, *Nature* **2012**, *486*, 43–51.
[16] A. Kraytsberg, Y. Ein-Eli, *Energy Fuels* **2014**, *28*, 7303–7330.
[17] S. Guo, S. Zhang, S. Sun, *Angew. Chem., Int. Ed.* **2013**, *52*, 8526–8544.
[18] C.-H. Cui, S.-H. Yu, *Acc. Chem. Res.* **2013**, *46*, 1427–1437.
[19] Y. Jiao, Y. Zheng, M. Jaroniec, S. Z. Qiao, *Chem. Soc. Rev.* **2015**, *44*, 2060–2086.
[20] X. Huang, Z. Zhao, L. Cao, Y. Chen, E. Zhu, Z. Lin, M. Li, A. Yan, A. Zettl, Y. M. Wang, X. Duan, T. Mueller, Y. Huang, *Science* **2015**, *348*, 1230–1234.
[21] L. Bu, S. Guo, X. Zhang, X. Shen, D. Su, G. Lu, X. Zhu, J. Yao, J. Guo, X. Huang, *Nat. Commun.* **2016**, *7*, 11850.
[22] L. Dai, Y. Xue, L. Qu, H.-J. Choi, J.-B. Baek, *Chem. Rev.* **2015**, *115*, 4823–4892.
[23] M. Zhou, H.-L. Wang, S. Guo, *Chem. Soc. Rev.* **2016**, *45*, 1273–1307.
[24] W. Niu, L. Li, X. Liu, N. Wang, J. Liu, W. Zhou, Z. Tang, S. Chen, *J. Am. Chem. Soc.* **2015**, *137*, 5555–5562.
[25] M. Liu, R. Zhang, W. Chen, *Chem. Rev.* **2014**, *114*, 5117–5160.
[26] W. Ding, L. Li, K. Xiong, Y. Wang, W. Li, Y. Nie, S. Chen, X. Qi, Z. Wei, *J. Am. Chem. Soc.* **2015**, *137*, 5414–5420.
[27] L. Xu, Q. Jiang, Z. Xiao, X. Li, J. Huo, S. Wang, L. Dai, *Angew Chem., Int. Ed.* **2016**, *55*, 5277–5281.
[28] Z. Tang, D. A. Robinson, N. Bokossa, B. Xu, S. Wang, G. Wang, *J. Am. Chem. Soc.* **2011**, *133*, 16037–16044.
[29] G. Li, R. Jin, *Acc. Chem. Res.* **2013**, *46*, 1749–1758.
[30] B. J. Hong, I. Eryazici, R. Bleher, R. V. Thaner, C. A. Mirkin, S. T. Nguyen, *J. Am. Chem. Soc.* **2015**, *137*, 8184–8191.
[31] J. Xie, Y. Zheng, J. Y. Ying, *J. Am. Chem. Soc.* **2009**, *131*, 888–889.
[32] R. M. Anderson, D. F. Yancey, L. Zhang, S. T. Chill, G. Henkelman, R. M. Crooks, *Acc. Chem. Res.* **2015**, *48*, 1351–1357.
[33] B. D. Briggs, M. R. Knecht, *J Phys Chem Lett* **2012**, *3*, 405–418.
[34] C.-L. Chen, N. L. Rosi, *Angew Chem., Int. Ed.* **2010**, *49*, 1924–1942.
[35] M. B. Dickerson, K. H. Sandhage, R. R. Naik, *Chem. Rev.* **2008**, *108*, 4935–4978.
[36] Y. Li, G. P. Whyburn, Y. Huang, *J. Am. Chem. Soc.* **2009**, *131*, 15998–15999.
[37] L. Ruan, C.-Y. Chiu, Y. Li, Y. Huang, *Nano Lett.* **2011**, *11*, 3040–3046.
[38] C.-Y. Chiu, Y. Li, L. Ruan, X. Ye, C. B. Murray, Y. Huang, *Nat. Chem.* **2011**, *3*, 393–399.
[39] N. Kröger, R. Deutzmann, M. Sumper, *Science* **1999**, *286*, 1129–1132.
[40] S. L. Sewell, D. W. Wright, *Chem. Mater.* **2006**, *18*, 3108–3113.
[41] K. E. Cole, A. N. Ortiz, M. A. Schoonen, A. M. Valentine, *Chem. Mater.* **2006**, *18*, 4592–4599.
[42] R. R. Naik, P. W. Whitlock, F. Rodriguez, L. L. Brott, D. D. Glawe, S. J. Clarson, M. O. Stone, *Chem. Commun.* **2003**, 238–239.
[43] R. Bhandari, M. R. Knecht, *ACS Catal.* **2011**, *1*, 89–98.
[44] R. Bhandari, M. R. Knecht, *Catal. Sci. Technol.* **2012**, *2*, 1360–1366.
[45] R. W. Murray, *Chem. Rev.* **2008**, *108*, 2688–2720.
[46] M.-C. Daniel, D. Astruc, *Chem. Rev.* **2004**, *104*, 293–346.
[47] O. Varnavski, G. Ramakrishna, J. Kim, D. Lee, T. Goodson, *J. Am. Chem. Soc.* **2010**, *132*, 16–17.
[48] R. Bhandari, D. B. Pacardo, N. M. Bedford, R. R. Naik, M. R. Knecht, *J. Phys. Chem. C* **2013**, *117*, 18053–18062.
[49] M. R. Knecht, D. W. Wright, *Chem. Commun.* **2003**, 3038–3039.
[50] D. F. Yancey, E. V. Carino, R. M. Crooks, *J. Am. Chem. Soc.* **2010**, *132*, 10988–10989.
[51] R. Lyyamperumal, L. Zhang, G. Henkelman, R. M. Crooks, *J. Am. Chem. Soc.* **2013**, *135*, 5521–5524.
[52] N. Ostojic, J. H. Thorpe, R. M. Crooks, *J. Am. Chem. Soc.* **2016**, *138*, 6829–6837.
[53] H. Ye, R. M. Crooks, *J. Am. Chem. Soc.* **2005**, *127*, 4930–4934.
[54] R. R. Adžić, S. Strbac, N. Anastasijević, *Mater. Chem. Phys.* **1989**, *22*, 349–375.
[55] N. M. Marković, T. J. Schmidt, B. N. Grgur, H. A. Gasteiger, R. J. Behm, P. N. Ross, *J. Phys. Chem. B* **1999**, *103*, 8568–8577.
[56] R. Li, Z. Wei, X. Gou, *ACS Catal.* **2015**, *5*, 4133–4142.
[57] G. He, Y. Song, K. Liu, A. Walter, S. Chen, S. Chen, *ACS Catal.* **2013**, *3*, 831–838.
[58] E. Higuchi, K. Hayashi, M. Chiku, H. Inoue, *Electrocatal.* **2012**, *3*, 274–283.
[59] Y. Li, W. Gao, L. Ci, C. Wang, P. M. Ajayan, *Carbon* **2010**, *48*, 1124–1130.
[60] J. Hernández, J. Solla-Gullón, E. Herrero, J. M. Feliu, A. Aldaz, *J. Nanosci. Nanotechnol.* **2009**, *9*, 2256–2273.
[61] H. Erikson, A. Sarapuu, K. Tammeveski, J. Solla-Gullón, J. M. Feliu, *ChemElectroChem* **2014**, *1*, 1338–1347.
[62] D. Li, C. Wang, D. S. Strmcnik, D. V. Tripkovic, X. Sun, Y. Kang, M. Chi, J. D. Snyder, D. van der Vliet, Y. Tsai, V. R. Stamenkovic, S. Sun, N. M. Markovic, *Energy Environ. Sci.* **2014**, *7*, 4061–4069.
[63] M. Subhramannia, V. K. Pillai, *J. Mater. Chem.* **2008**, *18*, 5858–5870.
[64] J.-Y. Ye, G. A. Attard, A. Brew, Z.-Y. Zhou, S.-G. Sun, D. J. Morgan, D. J. Willock, *J. Phys. Chem. C* **2016**, *120*, 7532–7542.
[65] K. Matsuzawa, T. Fukushima, M. Inaba, *Electrocatal.* **2010**, *1*, 169–177.

Submitted: September 20, 2016
Accepted: November 4, 2016